

# Production of $\Lambda_c^+$ hypernuclei in antiproton - nucleus collisions

R. Shyam<sup>a</sup>, K. Tsushima<sup>b</sup>

<sup>a</sup>*Saha Institute of Nuclear Physics, 1/AF Bidhan Nagar, Kolkata 700064, India*

<sup>b</sup>*Laboratório de Física Teórica e Computacional, Universidade Cruzeiro do Sul, Rua Galvão Bueno, 868, Liberdade 01506-000, São Paulo, SP, Brazil*

---

## Abstract

We investigate the production of charm-baryon hypernucleus  ${}^{16}_{\Lambda_c^+}\text{O}$  in the antiproton -  ${}^{16}\text{O}$  collisions within a fully covariant model that is based on an effective Lagrangian approach. The explicit  $\bar{\Lambda}_c^-\Lambda_c^+$  production vertex is described by the  $t$ -channel  $D^0$  and  $D^{*0}$  meson-exchanges in the initial collision of the incident antiproton with one of the protons of the target nucleus. The  $\Lambda_c^+$  bound state spinors as well as the self-energies of the exchanged mesons employed in our calculations are derived from the quark-meson coupling model. The parameters of various vertices are taken to be the same as those used in our previous study of the elementary  $\bar{p} + p \rightarrow \bar{\Lambda}_c^- + \Lambda_c^+$  reaction. We find that for antiproton beam momenta of interest to the  $\bar{P}ANDA$  experiment, the  $0^\circ$  differential cross sections for the formation of  ${}^{16}_{\Lambda_c^+}\text{O}$  hypernuclear states with simple particle-hole configurations, have magnitudes in the range of a few  $\mu\text{b}/\text{sr}$ .

*Keywords:* Production of  $\Lambda_c^+$  hypernuclei, antiproton-nucleus collisions, covariant production model, bound charm-baryon spinors from quark-meson coupling model

*PACS:* 14.20.Lq, 11.10.Ef, 12.39.Ki, 13.60.Rj

---

The investigation of the production of heavy flavor hadrons consisting of a charm-quark is of considerable interest as it provides an additional means for a better understanding of quantum chromodynamics (QCD) (see, e.g., Refs. [1, 2]). The future  $\bar{P}ANDA$  ("antiproton annihilation at Darmstadt") experiment at the under-construction antiproton and ion research facility (FAIR) in Darmstadt, Germany, includes a rich program on the measurements of the charm-meson and charm-baryon production in the antiproton

( $\bar{p}$ ) collisions with proton and nuclei at the beam momenta  $\leq 15$  GeV/c [3]. The accurate knowledge of the charm-meson  $\bar{D}D$  ( $\bar{D}^0D^0$  and  $D^-D^+$ ) production cross sections in these reactions, is important because the charmonium states above the open charm threshold will generally be identified by means of their decays to  $\bar{D}D$  channels unless this is forbidden by some conservation laws [4, 5].

Studies of the production and spectroscopy of charm-baryons (e.g.  $\Lambda_c^+$ ) are similarly interesting. Due to the presence of three quarks (two light and one heavy), the structure of the charm-baryon is more complicated. In contrast to the mesons, there can be more states as there are more possibilities of orbital excitations. At higher beam momenta of the  $\bar{p}$  at the  $\bar{P}ANDA$  facility the yields of the channels with charm-baryons exceeds those of the charm-meson channels by factors of 3-4, which is confirmed by calculations of the production of the ground state charm-baryon pair,  $\bar{\Lambda}_c^- \Lambda_c^+$  and the meson pairs  $\bar{D}D$  in the  $\bar{p}p$  collisions in Refs. [6, 7]. This is also seen in the calculations of the Jülich group [8, 9, 10]. In studies of the charm-baryon in the  $\bar{p}$ -proton (nucleus) reactions the production of extra particles is not needed for the charm conservation. This reduces the threshold energy as compared to the reactions induced by, say, proton.

Studies of the charm-meson and baryon production in the  $\bar{p}$ -nucleus collisions explore the properties of charm-hadrons in the nuclear medium and provide information about the charm-hadron-nucleon ( $N$ ) interaction in the nuclear medium [11, 12, 13].

The  $\Lambda_c^+ - N$  interaction has come in focus after discoveries of many exotic hadrons [e.g.  $X(3872)$ , and  $Z(4430)$ ] by the Belle experiments [14, 15]. These hadrons are considered to be either the 4-quark bound states including the charm one or the composite states of two (or more) hadrons (see, e.g., Ref. [16] for a review). There is no conclusive evidence for the existence of the two-body bound states in the  $\Lambda_c^+ - N$  channel. It will critically depend on the nature of the  $\Lambda_c^+ - N$  interaction. Since performing scattering experiments in this channel is not feasible in the foreseeable future, alternative methods will have to be explored for determining this interaction. Some effort has been made in this direction in the lattice QCD calculations by the HAL QCD collaboration [17], but their results are limited to pion masses around or in excess of 600 MeV. Another viable alternative is to study  $\Lambda_c^+$  hypernuclei that can be produced in the  $\bar{p}$  induced reactions on nuclei at the  $\bar{P}ANDA$  facility. In the past the study of the  $\Lambda$  hypernuclear states has provided important information about the  $\Lambda - N$  interaction (see, e.g., the reviews

[18, 19, 20]). Furthermore, in a theoretical study of the  $\Xi$ -hypernuclei, it has been shown that the properties of the states of such nuclei are strongly dependent on the nature of the  $\Xi - N$  interaction [21].

The existence of the  $\Lambda_c^+$  hypernuclei was predicted already in 1975 [22]. Since then several theoretical calculations have been reported for such nuclei that are based on the idea of the close similarity between the quark structures of  $\Lambda$  and  $\Lambda_c^+$ . They have predicted a rich spectrum of charm-hypernuclei spanning over a wide range of atomic mass numbers [23, 24, 25, 26, 27, 28, 29, 30]. However, there is a large variation in the binding energies and the potential depths predicted by these authors. More recently, in a series of publications [31, 32, 33, 34] systematic and quantitative studies of the  $\Lambda_c^+$  hypernuclei have been reported within the quark-meson coupling (QMC) model. These studies have predicted a number of states and their binding energies for the  $\Lambda_c^+$  hypernuclei,  ${}_{\Lambda_c^+}^{17}\text{O}$ ,  ${}_{\Lambda_c^+}^{41}\text{Ca}$ ,  ${}_{\Lambda_c^+}^{49}\text{Ca}$ ,  ${}_{\Lambda_c^+}^{91}\text{Zr}$ , and  ${}_{\Lambda_c^+}^{209}\text{Pb}$ . However, none of these references reports any production cross section for the formation of the  $\Lambda_c^+$  hypernuclei in an actual reaction.

In this letter, we present, for the first time, results for the cross sections of the  $\Lambda_c^+$  hypernuclear production in the  $\bar{p} - {}^{16}\text{O}$  collisions. We describe this reaction within an effective Lagrangian model (see, e.g. Refs. [21, 35, 36, 37, 38]), where  $\bar{\Lambda}_c^- \Lambda_c^+$  production takes place via  $t$ -channel exchanges of  $D^0$  and  $D^{*0}$  mesons in collisions of the  $\bar{p}$  with one of the protons of the target nucleus in the initial state [see, Figs. 1(a) and 1(b)]. The  $\Lambda_c^+$  is captured into one of the orbits of the residual nucleus to make the hypernucleus, while  $\bar{\Lambda}_c^-$  rescatters onto its mass shell [Fig. 1(a)]. The  $s$ - and  $u$ -channel resonance excitation diagrams are suppressed, as no resonance with energy in excess of 3.0 GeV having branching ratios for decay to the  $\Lambda_c^+$  channel is known. The direct  $\bar{p}p$  annihilation into  $\bar{\Lambda}_c^- \Lambda_c^+$  via the contact diagrams is also suppressed due to the Okubo-Zweig-Iizuka rule.

Our model retains the full field theoretic structure of the interaction vertices and treats baryons as Dirac particles. The  $\Lambda_c^+$  bound state spinors have been calculated within the QMC model. This provides an opportunity to investigate the role of the quark degrees of freedom in the charm-hypernuclear production, which involves larger momentum transfers to the target nucleus. Therefore, it appears a good case for examining such short distance effects. In the QMC model [39], quarks within the non-overlapping nucleon bags (modeled using the MIT bag), interact self-consistently with the isoscalar-scalar ( $\sigma$ ) and isoscalar-vector ( $\omega$ ) mesons in the mean field approximation. The

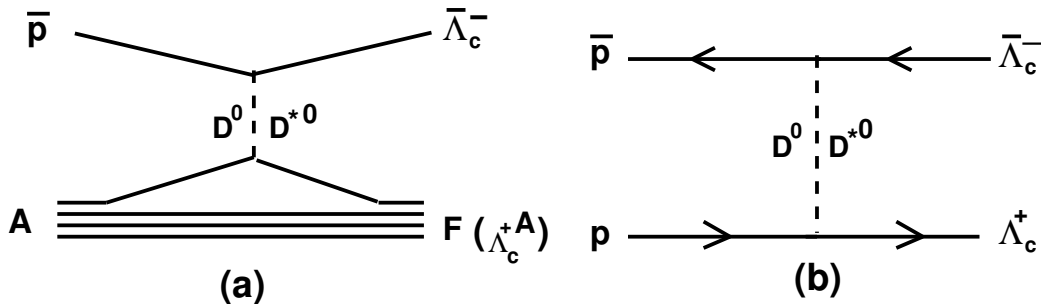


Figure 1: (a) Graphical representation of the model used to describe the charm-hypernuclear production reaction  $\bar{p}+A \rightarrow \bar{\Lambda}_c^-+F(=\Lambda_c^+A)$ .  $D^0$  and  $D^{*0}$  in the intermediate line represent the exchanges of  $D^0$  pseudoscalar and  $D^{*0}$  vector mesons, respectively. (b) The diagram to describe the elementary reaction  $\bar{p}+p \rightarrow \bar{\Lambda}_c^-+\Lambda_c^+$ . The arrows show the directions of the relative momenta.

explicit treatment of the nucleon internal structure represents an important departure from quantum hadrodynamics (QHD) [40]. The self-consistent response of the bound quarks to the mean  $\sigma$  field leads to a new saturation mechanism for nuclear matter [39]. The QMC model has been used to study the properties of finite nuclei [41], the binding of  $\omega$ ,  $\eta$ ,  $\eta'$  and  $D$  mesic nuclei [42, 43, 44] and also the effect of the medium on  $K^\pm$  and  $J/\Psi$  production [45].

For the evaluation of the amplitudes corresponding to the processes shown in Fig. 1(a), one requires the effective Lagrangians at the baryon-meson-nucleon vertices, and the propagators for the  $D^0$  and  $D^{*0}$  mesons. The masses of these mesons have been taken to be 1.867 GeV and 2.008 GeV, respectively. The denominators of these propagators involve the meson self-energies that account for the medium effects on their propagation through the nucleus.

The effective Lagrangians at the charm-baryon-meson-nucleon vertices have been adopted from Refs. [6, 46, 47, 48]. For the  $D^0$  meson-exchange vertices we have

$$\mathcal{L}_{D^0BN} = ig_{BD^0N}\bar{\psi}_B\gamma_5\psi_N\phi_{D^0} + H.c., \quad (1)$$

where  $\psi_B$  and  $\psi_N$  are the charm baryon and nucleon (antinucleon) fields, respectively, while  $\phi_{D^0}$  is the  $D^0$  meson field.  $g_{BD^0N}$  in Eq. (1) represents the vertex coupling constant at the charm-baryon(B)- $D^0$ -meson-nucleon (-antinucleon) vertex.

For the  $D^{*0}$  meson-exchange vertices, the effective Lagrangian is

$$\mathcal{L}_{D^{*0}BN} = g_{D^{*0}BN} \bar{\psi}_B \gamma_\mu \psi_N \theta_{D^{*0}}^\mu + \frac{f_{D^{*0}BN}}{4M} \bar{\psi}_B \sigma_{\mu\nu} \psi_N G_{D^{*0}}^{\mu\nu} + H.c., \quad (2)$$

where  $\theta_{D^{*0}}^\mu$  is the vector meson field, with field strength tensor  $G_{D^{*0}}^{\mu\nu} = \partial^\mu \theta_{D^{*0}}^\nu - \partial^\nu \theta_{D^{*0}}^\mu$ , and  $\sigma_{\mu\nu}$  is the usual tensor operator in the Dirac space. The vector and tensor couplings are defined by  $g$  and  $f$ , respectively, which were fixed in Refs. [47, 49, 50] by using the SU(4) symmetry arguments in the description of the exclusive charm-hadron production in  $\bar{D}N$  and  $DN$  scattering within an one-boson-exchange picture. As done in our study of the elementary reaction  $\bar{p} + p \rightarrow \bar{\Lambda}_c^- + \Lambda_c^+$  [6], the values of  $f$  and  $g$  at various vertices are adopted from Ref. [47], as  $g_{ND^0B} = 13.98$ ,  $g_{ND^{*0}B} = 5.64$  and  $f_{ND^{*0}B} = 18.37$ . For both the proton and the antiproton vertices, the same couplings were used. It was noted in Ref. [6] that the exchange of the  $D^{*0}$  meson dominates the  $\bar{\Lambda}_c^- \Lambda_c^+$  production in the  $\bar{p}p$  reaction even for beam momenta closer to the production threshold. Therefore, it is expected that this exchange mechanism will dominate the  $\Lambda_c^+$  hypernuclear production as well.

We use a monopole form factor to regulate the off-shell behavior of the vertices (see, e.g., Refs. [51, 52])

$$F_i(q_i) = \frac{\lambda_i^2 - m_{D_i}^2}{\lambda_i^2 - q_{D_i}^2}, \quad (3)$$

where  $q_{D_i}$  is the momentum of the  $i$ -th exchanged meson with mass  $m_{D_i}$ , and  $\lambda_i$  is the corresponding cutoff parameter, which governs the range of suppression of the contributions of high momenta carried out via the form factor. As was done in Ref. [6], we chose a value of 3.0 GeV for  $\lambda_i$  at both the vertices. The same  $\lambda_i$  was also used in the studies of  $\bar{D}D$  production in antiproton-proton and antiproton-nucleus collisions in Refs. [7] and [11], respectively, within a similar type of the effective Lagrangian model.

The propagators for the  $D^0$  and  $D^{*0}$  mesons are given by

$$G_{D^0}(q_{D^0}) = \frac{i}{q_{D^0}^2 - m_{D^0}^2 - \Pi_{D^0}}, \quad (4)$$

$$G_{D^{*0}}^{\mu\nu}(q_{D^{*0}}) = -i \left( \frac{g^{\mu\nu} - q_{D^{*0}}^\mu q_{D^{*0}}^\nu / q_{D^{*0}}^2}{q_{D^{*0}}^2 - (m_{D^{*0}} - i\Gamma_{D^{*0}}/2)^2 - \Pi_{D^{*0}}} \right), \quad (5)$$

where  $q_{D^0}$  and  $q_{D^{*0}}$  are the four-momenta of  $D^0$  and  $D^{*0}$  mesons, respectively, while  $m_{D^0}$  and  $m_{D^{*0}}$  are their masses.  $\Pi_{D^0}$  and  $\Pi_{D^{*0}}$  represent the (complex)

self-energies of  $D^0$  and  $D^{*0}$  mesons, respectively. In Eq. (5),  $\Gamma_{D^{*0}}$  is the total width of the  $D^{*0}$  meson, which is about 2.0 MeV according to the latest particle data group estimate [53].

In this exploratory study, the self-energies  $\Pi_{D^0}$  and  $\Pi_{D^{*0}}$  have been obtained from the mean-field potentials for  $D^0$  and  $D^{*0}$  mesons in  $^{16}\text{O}$  calculated self-consistently within the QMC model in the local density approximation as described in Ref. [44]. The self-energy is related to the potential by  $\Pi_{D_i} = 2\omega_{D_i}U_{D_i}(q_{D_i})$ , where  $\omega_{D_i} = \sqrt{q_{D_i}^2 + m_{D_i}^2}$ , and  $U_{D_i}$  is the potential in the momentum space of meson  $D_i$ , with  $D_i$  standing for  $D^0$  or  $D^{*0}$ .

After having established the effective Lagrangians, coupling constants, and forms of the propagators, the amplitudes of  $D^0$  and  $D^{*0}$  exchange diagrams can be written by following the Feynman rules. The signs of these amplitudes are fixed by those of the effective Lagrangians, the coupling constants, and the propagators as described above. These signs are not allowed to change anywhere in the calculations.

At the upper vertices of Fig. 1(a), the amplitudes involve free-space spinors of the antiparticles, while at the lower vertices, they have spinors for bound proton in the initial state (to be represented by  $\psi(k_p)$ ) and bound  $\Lambda_c^+$  in the final state (to be represented by  $\psi(k_{\Lambda_c^+})$ ). These are the four component Dirac spinors, which are solutions of the Dirac equation for a bound state problem in the presence of external potential fields. They are calculated within the QMC model as described below. We write

$$\psi(k_i) = \delta(k_{i0} - E_i) \begin{pmatrix} f(K_i)\mathcal{Y}_{\ell 1/2 j}^{m_j}(\hat{k}_i) \\ -ig(K_i)\mathcal{Y}_{\ell' 1/2 j}^{m_j}(\hat{k}_i) \end{pmatrix}. \quad (6)$$

In our notation  $k_i$  represents a four momentum, and  $\mathbf{k}_i$  a three momentum. The magnitude of  $\mathbf{k}_i$  is represented by  $K_i$ , and its directions by  $\hat{k}_i$ .  $k_{i0}$  represents the timelike component of momentum  $k_i$ . In Eq. (6),  $f(K_i)$  and  $g(K_i)$  are the radial parts of the upper and lower components of the spinor  $\psi(k_i)$  with  $i$  representing either a proton or a  $\Lambda_c^+$ . The coupled spherical harmonics,  $\mathcal{Y}_{\ell 1/2 j}^{m_j}$ , is given by

$$\mathcal{Y}_{\ell 1/2 j}^{m_j}(\hat{k}_i) = \langle \ell m_\ell 1/2 \mu | j m_j \rangle Y_{\ell m_\ell}(\hat{k}_i) \chi_\mu, \quad (7)$$

where  $Y_{\ell m_\ell}$  represents the spherical harmonics, and  $\chi_\mu$  the spin-space wave function of a spin- $\frac{1}{2}$  particle. In Eq. (6)  $\ell' = 2j - \ell$  with  $\ell$  and  $j$  being the orbital and total angular momenta, respectively.

To calculate the spinors for the final bound charm-hypernuclear state and the initial proton bound state within the QMC model, we construct a simple, relativistic shell model, with the nucleon core calculated in a combination of self-consistent scalar and vector mean fields. The Lagrangian density for a hypernuclear system in the QMC model is written as a sum of two terms,

$$\mathcal{L}_{QMC}^{HY} = \mathcal{L}_{QMC}^N + \mathcal{L}_{QMC}^Y, \quad (8)$$

$$\begin{aligned} \mathcal{L}_{QMC}^N &\equiv \bar{\psi}_N(\mathbf{r}) \left[ i\gamma \cdot \partial - M_N^*(\sigma) - (g_\omega \omega(\mathbf{r}) + g_\rho \frac{\tau_3^N}{2} b(\mathbf{r}) + \frac{e}{2}(1 + \tau_3^N)A(\mathbf{r}))\gamma_0 \right] \psi_N(\mathbf{r}) \\ &\quad - \frac{1}{2}[(\nabla\sigma(\mathbf{r}))^2 + m_\sigma^2\sigma(\mathbf{r})^2] + \frac{1}{2}[(\nabla\omega(\mathbf{r}))^2 + m_\omega^2\omega(\mathbf{r})^2] \\ &\quad + \frac{1}{2}[(\nabla b(\mathbf{r}))^2 + m_\rho^2 b(\mathbf{r})^2] + \frac{1}{2}(\nabla A(\mathbf{r}))^2, \end{aligned} \quad (9)$$

$$\begin{aligned} \mathcal{L}_{QMC}^Y &\equiv \bar{\psi}_Y(\mathbf{r}) [i\gamma \cdot \partial - M_Y^*(\sigma) - (g_\omega^Y \omega(\mathbf{r}) + g_\rho^Y I_3^Y b(\mathbf{r}) + eQ_Y A(\mathbf{r}))\gamma_0] \psi_Y(\mathbf{r}), \\ &\quad (Y = \Lambda, \Sigma^{0,\pm}, \Xi^{0,+}, \Lambda_c^+, \Sigma_c^{0,+,++}, \Xi_c^{0,+}, \Lambda_b), \end{aligned} \quad (10)$$

where  $\psi_N(\mathbf{r})$  and  $\psi_Y(\mathbf{r})$  are the nucleon and the hyperon (strange, charm or bottom baryon) fields, respectively.  $A(r)$  is the Coulomb field.  $g_\omega$  and  $g_\rho$  are the  $\omega$ -N and  $\rho$ -N coupling constants which are related to the corresponding ( $u, d$ ) quark- $\omega$ ,  $g_\omega^q$ , and ( $u, d$ ) quark- $\rho$ ,  $g_\rho^q$ , coupling constants, as  $g_\omega = 3g_\omega^q$  and  $g_\rho = g_\rho^q$ .  $I_3^Y$  and  $Q_Y$  are the third component of the hyperon isospin operator and its electric charge in units of the proton charge,  $e$ , respectively.

The following set of equations of motion are obtained for the hypernuclear system from the Lagrangian densities defined by Eqs. (9)-(10),

$$[i\gamma \cdot \partial - M_N(\sigma) - (g_\omega \omega(\mathbf{r}) + g_\rho \frac{\tau_3^N}{2} b(\mathbf{r}) + \frac{e}{2}(1 + \tau_3^N)A(\mathbf{r}))\gamma_0] \psi_N(\mathbf{r}) = 0, \quad (11)$$

$$[i\gamma \cdot \partial - M_Y(\sigma) - (g_\omega^Y \omega(\mathbf{r}) + g_\rho^Y I_3^Y b(\mathbf{r}) + eQ_Y A(\mathbf{r}))\gamma_0] \psi_Y(\mathbf{r}) = 0, \quad (12)$$

$$(-\nabla_r^2 + m_\sigma^2)\sigma(\mathbf{r}) = g_\sigma C_N(\sigma)\rho_s(\mathbf{r}) + g_\sigma^Y C_Y(\sigma)\rho_s^Y(\mathbf{r}), \quad (13)$$

$$(-\nabla_r^2 + m_\omega^2)\omega(\mathbf{r}) = g_\omega \rho_B(\mathbf{r}) + g_\omega^Y \rho_B^Y(\mathbf{r}), \quad (14)$$

$$(-\nabla_r^2 + m_\rho^2)b(\mathbf{r}) = \frac{g_\rho}{2}\rho_3(\mathbf{r}) + g_\rho^Y I_3^Y \rho_B^Y(\mathbf{r}), \quad (15)$$

$$(-\nabla_r^2)A(\mathbf{r}) = e\rho_p(\mathbf{r}) + eQ_Y \rho_B^Y(\mathbf{r}), \quad (16)$$

where,  $\rho_s(\mathbf{r})$  ( $\rho_s^Y(\mathbf{r})$ ),  $\rho_B(\mathbf{r})$  ( $\rho_B^Y(\mathbf{r})$ ),  $\rho_3(\mathbf{r})$  and  $\rho_p(\mathbf{r})$  are the scalar, baryon, third component of isovector, and proton densities at position  $\mathbf{r}$  in the hypernucleus [42]. On the right hand side of Eq. (13), a new and characteristic feature of the QMC model appears that arises from the internal structures of the

Table 1: Binding energies of  $\Lambda_c^+$  and  $p$  for each shell as predicted by the QMC model.

| State   | BE<br>(MeV) |
|---|-------------|
| ${}_{\Lambda_c^+}^{16}\text{O}(\Lambda_c^+ 0p_{1/2})$ | 7.17        |
| ${}_{\Lambda_c^+}^{16}\text{O}(\Lambda_c^+ 0p_{3/2})$ | 7.20        |
| ${}_{\Lambda_c^+}^{16}\text{O}(\Lambda_c^+ 0s_{1/2})$ | 12.78       |
| ${}^{16}\text{O}(p 0p_{1/2})$                         | 11.87       |

nucleon and hyperon, namely,  $g_\sigma C_N(\sigma) = -\frac{\partial M_N(\sigma)}{\partial \sigma}$  and  $g_\sigma^Y C_Y(\sigma) = -\frac{\partial M_Y(\sigma)}{\partial \sigma}$  where  $g_\sigma \equiv g_\sigma(\sigma = 0)$  and  $g_\sigma^Y \equiv g_\sigma^Y(\sigma = 0)$ . We use the nucleon and hyperon masses to calculate  $C_{N,Y}(\sigma)$  employing the parameters of QMC-I summarized in table 13 of Ref. [45]. The scalar and vector fields as well as the spinors for hyperons and nucleons, can be obtained by solving these coupled equations self-consistently.

We note here that, for the Dirac equation for  $\Lambda_c^+$  baryon [Eq. (12)], the effects of Pauli blocking at the quark level, is introduced by adding a repulsive potential. This is the same as that used for the  $\Lambda$ -hyperon case. This was extracted by the fit to the  $\Lambda$ - and  $\Sigma$ -hypernuclei taking into account the  $\Sigma N - \Lambda N$  channel coupling [32, 33, 34, 43]. The modified Dirac equation for the  $\Lambda_c^+$  baryon is,

$$[i\boldsymbol{\gamma} \cdot \boldsymbol{\partial} - M_Y(\sigma) - (\lambda_{\Lambda_c^+} \rho_B(\mathbf{r}) + g_\omega^Y \omega(\mathbf{r}) + g_\rho I_3^Y b(\mathbf{r}) + eQ_Y A(\mathbf{r}))\gamma_0]\psi_Y(\mathbf{r}) = 0, \quad (17)$$

where  $\rho_B(\mathbf{r})$  is the baryon density at the position  $\mathbf{r}$  in the  $\Lambda_c^+$ -hypernucleus. The value of  $\lambda_{\Lambda_c^+}$  is  $60.25 \text{ MeV (fm)}^3$ . The details about the effective Pauli blocking at the quark level can be found in Refs. [43, 45].

We have chosen the reaction  $\bar{p} + {}^{16}\text{O} \rightarrow \bar{\Lambda}_c^- + {}_{\Lambda_c^+}^{16}\text{O}$  for the first numerical application of our model of charm-hypernuclear production. The target nucleus is a doubly closed system. The QMC model predicts three bound states for the charm-hypernucleus  ${}_{\Lambda_c^+}^{16}\text{O}$ . The predicted quantum numbers and binding energies of these states are shown in Table 1. We assume the initial bound proton state to have quantum numbers of the outermost  $0p_{1/2}$  proton orbit of the target nucleus. The predicted binding energy of this state by QMC is also shown in Table 1. The hypernuclear spectrum is clearly divided into three groups corresponding to the configurations  $(0p_{1/2}^{-p}, 0s_{1/2}^{\Lambda_c^+})$ ,

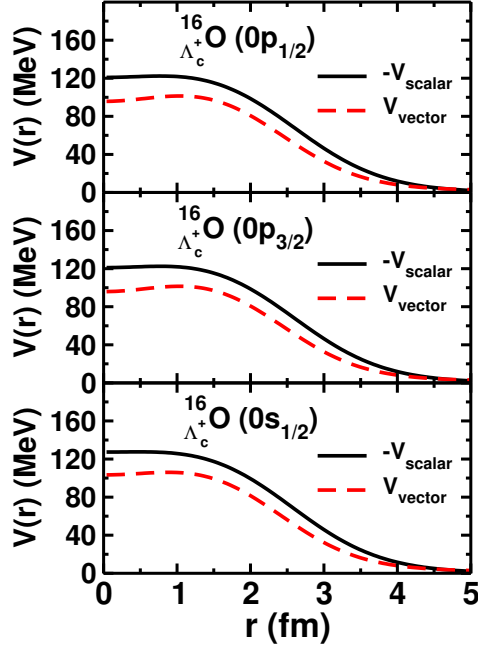


Figure 2: (color online) Vector and scalar potential fields felt by  $\Lambda_c^+$  for  $0p_{1/2}$ ,  $0p_{3/2}$  and  $0s_{1/2}$   $\Lambda_c^+$  states in  $^{16}_{\Lambda_c^+}\text{O}$ , where the vector potential field strength contains the effective Pauli blocking potential for each state of  $\Lambda_c^+$  [see Eq. (17)].

$(0p_{1/2}^{-p}, 0p_{1/2}^{\Lambda_c^+})$ , and  $(0p_{1/2}^{-p}, 0p_{3/2}^{\Lambda_c^+})$ . Since  $0p_{3/2}$  proton hole state has a much larger binding energy, any configuration mixing is expected to be negligible and has not been considered in this study.

In Fig. 2, we show the scalar and vector fields as calculated within the QMC model for  $0p_{1/2}$ ,  $0p_{3/2}$  and  $0s_{1/2}$   $\Lambda_c^+$  states, where the strength of the vector field contains also the effective Pauli blocking potential for each state of  $\Lambda_c^+$  (see Eq. (17)). It may be recalled that in the QMC model the scalar and vector fields are generated by the couplings of the  $\sigma$  and  $\omega$  mesons to the quarks. Due to the different masses of these mesons and their couplings, especially the density dependence or non-linear dependence of the  $\sigma N$  and  $\sigma \Lambda_c^+$  coupling strengths due to the baryon internal structure, the scalar and vector fields may acquire non-trivial radial dependence. This is in contrast to a phenomenological model where scalar and vector fields have the same Woods-Saxon (WS) radial form (see, e.g., Ref. [21]). In any case, because in such models the depths of these fields are searched to reproduce the ex-

perimental binding energies of a given state, they can not be applied at this stage to  $\Lambda_c^+$  bound states due lack of any experimental information about them. In Fig. 2, we note that sum of the scalar and vectors fields at  $r = 0$  is about -30 MeV for all the three states. This is roughly equivalent to the depth of a non-relativistic potential at this point. This is about 15 MeV less (in absolute value) than the depth of the  $\Lambda_c^+$  -  $^{16}\text{O}$  Hartree potential calculated in Ref. [24]. Therefore, relativistic self-consistent procedure has its consequences.

Figs. 3(a) and 3(b) show the moduli of the upper and lower components of  $0p_{1/2}$ ,  $0p_{3/2}$  and  $0s_{1/2}$   $\Lambda_c^+$  spinors for the  $^{16}_{\Lambda_c^+}\text{O}$  charm-hypernucleus in coordinate space and momentum space, respectively. The spinors in the momentum space are obtained by Fourier transformation of the corresponding coordinate space spinors. We note that only for  $K_{\Lambda_c^+} < \text{approximately } 1.0 \text{ fm}^{-1}$ , are the magnitudes of the lower components ( $|g(K_{\Lambda_c^+})|$ ) substantially smaller than those of the upper components ( $|f(K_{\Lambda_c^+})|$ ). In the region of  $K_{\Lambda_c^+}$  pertinent to the charm-hypernuclear production,  $|g(K_{\Lambda_c^+})|$  may not be negligible.

To get the  $T$ -matrix of the reaction of the process shown in Fig. 1(a), one has to integrate the amplitudes corresponding to each meson-exchange graph over the independent intermediate momenta  $k_p$  and  $k_{\Lambda_c^+}$  subject to the constraints imposed by the momentum conservation at each vertex.

We have used plane waves to describe the motions of the  $\bar{p}$  and  $\bar{\Lambda}_c^-$  baryon in the entrance and outgoing channels, respectively. However, initial- and final-state interactions are approximately accounted for within an eikonal-approximation based procedure [36] that was used in Refs. [11] to describe the charm-meson production in the  $\bar{p}$ -nucleus reactions. In this work we have employed the same parameters as those of Ref. [11] to estimate the distortion effects in the initial and final channels.

The threshold momentum for the production of  $^{16}_{\Lambda_c^+}\text{O}$  in  $\bar{p}$  induced reaction on  $^{16}\text{O}$  is about 3.953 GeV/c, while that for the  $\bar{\Lambda}_c^- + \Lambda_c^+$  production in the elementary  $\bar{p} + p$  reaction is 10.162 GeV/c. The shift in the threshold of the hypernuclear production reaction to lower beam momenta is mainly due to the Fermi motion effects. Therefore,  $\Lambda_c^+$  hypernuclear production experiments may be feasible even in the beginning stage of the FAIR project when  $\bar{p}$  beam momenta may be lower than their maximum planned value of 15 GeV/c.

In Fig. 4, we show the  $0^\circ$  differential cross sections  $[(d\sigma/d\Omega)_0]$  for the reaction  $\bar{p} + ^{16}\text{O} \rightarrow \bar{\Lambda}_c^- + ^{16}_{\Lambda_c^+}\text{O}$  obtained by using the proton-hole and  $\Lambda_c^+$  bound

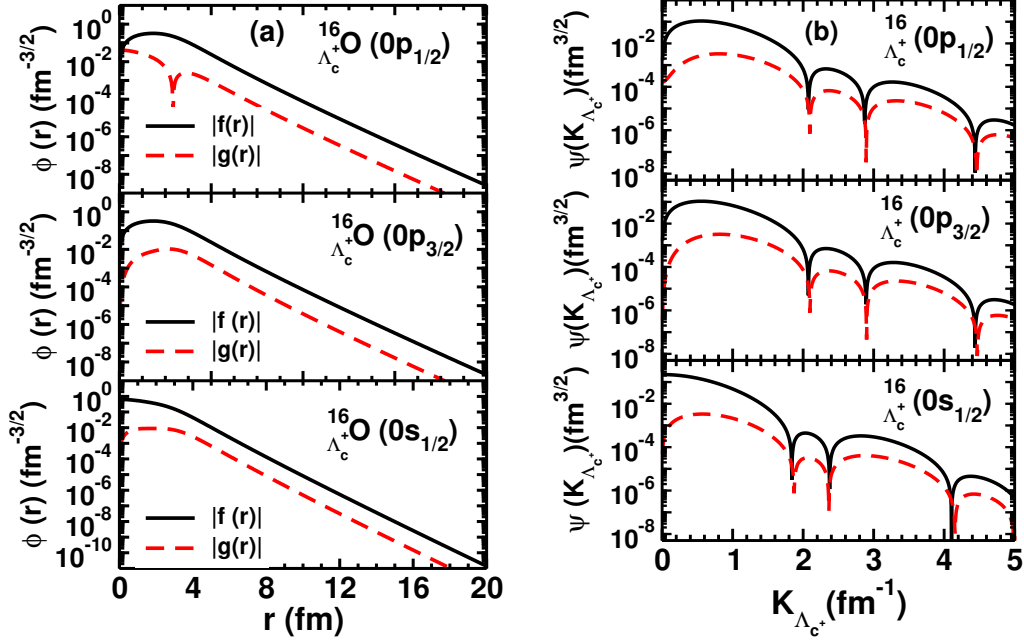


Figure 3: (color online) (a) Moduli of the upper ( $|f(r)|$ ) and lower ( $|g(r)|$ ) components of the coordinate space spinors for  $0p_{1/2}$ ,  $0p_{3/2}$  and  $0s_{1/2}$   $\Lambda_c^+$  states in  $^{16}_{\Lambda_c^+}\text{O}$ . Solid lines represent the upper component while the dashed line the lower component. (b) Moduli of upper (solid lines) and lower (dashed lines) components of the momentum space spinors of the  $\Lambda_c^+$  bound states in  $^{16}_{\Lambda_c^+}\text{O}$  for the same states as in the left panel.

state spinors calculated within the QMC model. Cross sections are shown for  $\bar{p}$  beam momenta in the range of threshold to 20 GeV/c. The charm-hypernuclear states populated are  $1^-$  and  $0^-$ ,  $1^+$  and  $0^+$ , and  $2^+$  and  $1^+$  corresponding to the particle-hole configurations  $(0p_{1/2}^{-p}, 0s_{1/2}^{\Lambda_c^+})$ ,  $(0p_{1/2}^{-p}, 0p_{1/2}^{\Lambda_c^+})$ , and  $(0p_{1/2}^{-p}, 0p_{3/2}^{\Lambda_c^+})$ , respectively. Cross sections to the higher  $J$  state of each configuration are shown in Fig. 4(a), while those to lower  $J$  in Fig. 4(b). We see that for each particle-hole configuration, the state with higher  $J$  has larger cross section. While for beam momenta  $\geq 8$  GeV/c, the cross-sections for states belonging to the  $(0p_{1/2}^{-p}, 0s_{1/2}^{\Lambda_c^+})$  configuration are larger than those of the other two configurations, for  $p_{\bar{p}}$  lower than 8 GeV/c those for states belonging to the  $(0p_{1/2}^{-p}, 0p_{1/2}^{\Lambda_c^+})$  configuration have larger values. However, the maximum difference between the cross sections of the states belonging to two configurations is not more than a factor of 1.4. The  $[(d\sigma/d\Omega)_0]$ , for the

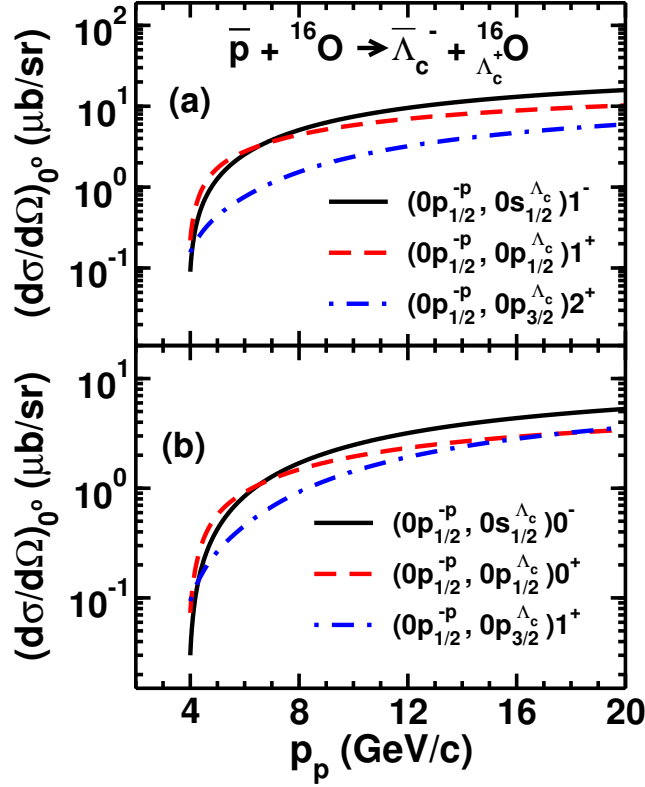


Figure 4: (color online) (a) Differential cross sections at  $0^\circ$  of the  $\bar{p} + {}^{16}\text{O} \rightarrow \bar{\Lambda}_c^- + {}^{16}_{\Lambda_c^+}\text{O}$  reaction leading to the  ${}^{16}_{\Lambda_c^+}\text{O}$  hypernuclear states of larger  $J$  value of each particle-hole configuration as indicated. (b) The same as in (a) but for states of lower  $J$  value of each configuration as indicated. In the legends  $\Lambda_c$  corresponds to  $\Lambda_c^+$ .

states belonging to the configuration  $(0p_{1/2}^{-p}, 0p_{3/2}^{\Lambda_c^+})$  are smaller than those of the  $(0p_{1/2}^{-p}, 0p_{1/2}^{\Lambda_c^+})$  configuration by factors of approximately 1.4 - 3.0.

It is to be noted that for  $\bar{p}$  beam momenta between 8 - 15 GeV/c (which are of interest to  $\bar{P}ANDA$  experiment) the magnitudes of the  $0^\circ$  differential cross sections vary between 1.5 - 3.8  $\mu\text{b}/\text{sr}$ , and 5.0 - 11.0  $\mu\text{b}/\text{sr}$  for states  $0^-$  and  $1^-$ , respectively, of the configuration  $(0p_{1/2}^{-p}, 0s_{1/2}^{\Lambda_c^+})$ . On the other hand, for states  $1^+$  and  $2^+$  of the configuration  $(0p_{1/2}^{-p}, 0p_{3/2}^{\Lambda_c^+})$ , it varies between 0.9 - 2.8  $\mu\text{b}/\text{sr}$ , and 1.6 - 6.0  $\mu\text{b}/\text{sr}$ , respectively. Furthermore, the cross sections for all the states consist almost solely of the contributions from the  $D^{*0}$  meson-

exchange process, with  $D^0$  meson-exchange terms being very small. This is similar to what has been noted in the case of the elementary  $\bar{p}+p \rightarrow \bar{\Lambda}_c^- + \Lambda_c^+$  reaction in Ref. [6]. The domination of the  $D^{*0}$  exchange process has been traced to the strong tensor coupling term of the  $D^{*0}$  meson couplings.

We, however, add that a major source of uncertainty in our results is provided by our treatment of initial- and final-state interactions. We use an eikonal-approximation based phenomenological method to account for these effects. Although the parameters of our method, namely, the antiproton-proton total cross section and the radius parameter of the target nucleus are independently determined by other authors by different methods, the lack of any experimental information to constrain them does not allow a thorough test of our model. Therefore, the absolute magnitude of our cross sections may have uncertainties. Furthermore, our treatment necessarily assumes that the shapes of the angular distributions are not affected by the distortion effects. This may change in a more rigorous treatment of the distortion effects that include both absorption and dispersion effects.

In summary, we have calculated the  $0^\circ$  differential cross sections for the production of the charm-hypernucleus  ${}^{16}_{\Lambda_c^+}\text{O}$  in the antiproton -  ${}^{16}\text{O}$  collisions within a covariant model. This is for the first time that cross sections of any kind have been calculated for the charm-baryon hypernuclear production within any model. In our calculations,  $\bar{\Lambda}_c^- \Lambda_c^+$  production takes place via the  $t$ -channel exchanges of  $D^0$  and  $D^{*0}$  mesons in the initial collisions of the  $\bar{p}$  with a target proton.  $\Lambda_c^+$  gets captured into one of the nuclear orbits while  $\bar{\Lambda}_c^-$  goes out.  $\Lambda_c^+$  bound state spinors are derived from the quark-meson coupling model. The coupling constants at the meson exchange vertices are taken to be the same as those used in a previous study of the elementary  $\bar{p} + p \rightarrow \bar{\Lambda}_c^- + \Lambda_c^+$  reaction by one of us [6]. The off-shell corrections at the vertices are accounted for by introducing monopole form factors with a cut-off parameter of 3.0 GeV, which is the same as that used in Ref. [6].

At beam momenta of interest to the  $\bar{P}ANDA$  experiment, the  $0^\circ$  differential cross section for the  $\bar{p} + {}^{16}\text{O} \rightarrow \bar{\Lambda}_c^- + {}^{16}_{\Lambda_c^+}\text{O}$  reaction varies between 0.9  $\mu\text{b}/\text{sr}$  to 11  $\mu\text{b}/\text{sr}$  depending on the final  $\Lambda_c^+$  state excited in the reaction. The relatively larger cross sections and low threshold for the production of the  ${}^{16}_{\Lambda_c^+}\text{O}$  hypernuclear states in the  $\bar{p}$  -  ${}^{16}\text{O}$  reaction may make it possible to perform such experiments at the  $\bar{P}ANDA$  facility even in the beginning stage of the FAIR facility.

This work has been supported by the Science and Engineering Research

Board (SERB), Department of Science and Technology, Government of India under Grant no. SB/S2/HEP-024/2013, and by Fundação de Amparo à Pesquisa do Estado de São Paulo (FAPESP), Brazil, Grants No. 2016/04191-3, and, No. 2015/17234-0, and Conselho Nacional de Desenvolvimento Científico e Tecnológico (CNPq), Grants No. 400826/2014-3 and No. 308088/2015-8.

## References

- [1] M. Neubert, Phys. Rep. **245** (1994) 259.
- [2] J. G. Körner, M. Krämer, and D. Pirjol, Prog. Part. Nucl. Phys. **33** (1994) 787.
- [3] W. Erni *et al.*, arXiv:0903.3905 [hep-ex].
- [4] U. Wiedner, Prog. Part. Nucl. Phys. **66** (2011) 477
- [5] E. Prencipe, Eur. Phys. J. Web. Conf. **95** (2015) 04052.
- [6] R. Shyam and H. Lenske, Phys. Rev. D **90** (2014) 014017.
- [7] R. Shyam and H. Lenske, Phys. Rev. D **93** (2016) 034016.
- [8] J. Haidenbauer, and G. Krein, Phys. Lett. B **678** (2010) 314.
- [9] J. Haidenbauer, and G. Krein, Phys. Rev. D **89**, (2014) 114003.
- [10] J. Haidenbauer, and G. Krein, Phys. Rev. D **91** (2015) 114022.
- [11] R. Shyam and K. Tsushima, Phys. Rev. D. **94** (2016) 074041.
- [12] A. Hosaka, T. Hyodo, K. Sudoh, Y. Yamaguchi and S. Yasui, arXiv:1606.08685 [hep-ph]
- [13] J. Yamagata-sekihara, C. Garcia-Recio, J. Nieves, L. L. Salcedo, and L. Tolos, Phys. Lett. **B 754** (2016) 26.
- [14] S. K. Choi et al. (Belle Collaboration), Phys. Rev. Lett. **91** (2003) 262001.
- [15] S. K. Choi et al. (Belle Collaboration), Phys. Rev. Lett. **100** (2008) 142001.

- [16] S. Godfrey and S. L. Olsen, *Ann. Rev. Nucl. Part. Sci.* **58** (2008) 51.
- [17] T. Miyamoto (for HAL QCD collaboration), arXiv:1602.07797 [hep-lat]
- [18] O. Hasimoto and H. Tamura, *Prog. Part. Nucl. Phys.* **57** (2006) 564.
- [19] R. Shyam, *Prog. Part. Nucl. Phys.* **61** (2008) 212.
- [20] A. Gal, E.V. Hungerford and D.J. Millener, *Rev. Mod. Phys.* **88** (2016) 035004.
- [21] R. Shyam, K. Tsushima, and A. W. Thomas, *Nucl. Phys.* **A881** (2012) 255.
- [22] A. A. Tyapkin, *Sov. J. Nucl. Phys.* **22** (1975) 181.
- [23] S. Iwato, *Lett. Nuovo Cim.* **19** (1977) 647.
- [24] C. B. Dover and S. H. Kahana, *Phys. Rev. Lett.* **39** (1977) 1506.
- [25] R. Gatto and F. Paccanoni, *Nuovo Cim.* **A46** (1978) 313.
- [26] N. N. Kolesnikov et al., *Sov. J. Nucl. Phys.* **34** (1981) 533.
- [27] G. Bhamathi, *Phys. Rev. C* **24** (1981) 1816.
- [28] H. Bando and M. Bando, *Phys. Lett.* **B109** (1982) 164.
- [29] B. F. Gibson, C. B. Dover, G. Bhamathi, and D. R. Lehman, *Phys. Rev. C* **27** (1983) 2085.
- [30] C. H. Cai, L. Li, Y. H. Tan, P. Z. Ning, *Europhys. Lett.* **64** (2003) 448.
- [31] K. Tsushima and F. C. Khanna, *Phys. Lett.* **B552** (2003) 138.
- [32] K. Tsushima and F. C. Khanna, *Phys. Rev. C* **67** (2003) 015211.
- [33] K. Tsushima and F. C. Khanna, *Prog. Theo. Phys. Suppl.* **149** (2003) 149.
- [34] K. Tsushima and F. C. Khanna, *J. Phys. G: Nucl. Part. Phys.* **30** (2004) 1765.
- [35] R. Shyam, H. Lenske and U. Mosel, *Phys. Rev. C* **69** (2004) 065205.

- [36] R. Shyam, H. Lenske and U. Mosel, Nucl. Phys. **A764** (2006) 313.
- [37] R. Shyam, K. Tsushima and A. W. Thomas, Phys. Lett. **B676** (2009) 51.
- [38] S. Bender, R. Shyam and H. Lenske, Nucl. Phys. **A 839** (2010) 51.
- [39] P. A. M. Guichon, Phys. Lett. **B200** (1988) 235.
- [40] B. D. Serot and J. D. Walecka, Adv. Nucl. Phys. **16** (1986) 1; *ibid*, Int. J. Mod. Phys. **E 6** (1997) 515.
- [41] K. Saito, K. Tsushima and A. W. Thomas, Nucl. Phys. **A609** (1996) 339.
- [42] K. Tsushima, D. H. Lu, A. W. Thomas, and K. Saito, Phys. Lett. **B443** (1998) 26.
- [43] K. Tsushima, K. Saito, J. Haidenbauer and A. W. Thomas, Nucl. Phys. **A630** (1998) 691.
- [44] K. Tsushima, D. H. Lu, A. W. Thomas, K. Saito R. H. Landau, Phys. Rev. C **59** (1999) 2824.
- [45] K. Saito, K. Tsushima and A. W. Thomas, Prog. Part. Nucl. Phys. **58** (2007) 1.
- [46] A. Müller-Groeling, K. Holinde, and J. Speth, Nucl. Phys. **A513** (1990) 557.
- [47] J. Haidenbauer, G. Krein, U.-G. Meissner, and L. Tolos, Eur. Phys. J. A **47** (2011) 18.
- [48] T. J. Hobbs, J. T. Londergan, and W. Melnitchouk, Phys. Rev. D **89** (2014) 074008.
- [49] J. Haidenbauer, G. Krein, U.-G. Meissner, and A. Sibirtsev, Eur. Phys. J. A **33** (2007) 107.
- [50] J. Haidenbauer, G. Krein, U.-G. Meissner, and A. Sibirtsev, Eur. Phys. J. A **37** (2008) 55.
- [51] R. Shyam, Phys. Rev. C **60** (1999) 055213.

- [52] R. Shyam and U. Mosel, Phys. Rev. C **67** (2003) 065202.
- [53] K. A. Olive *et al.* (Particle Data Group), Chin. Phys. C **38** (2014) 090001.